Evaluation of Bi–W–Oxides for Visible Light Photocatalysis

ARTICLE *in* PHYSICA STATUS SOLIDI (A) APPLICATIONS AND MATERIALS · FEBRUARY 2006

Impact Factor: 1.62 · DOI: 10.1002/pssa.200521129

5 AUTHORS, INCLUDING:

V. N. Tsaneva
University of Cambridge
62 PUBLICATIONS **350** CITATIONS

SEE PROFILE

Original Paper

phys. stat. sol. (a) **203**, No. 2, 327–335 (2006) / **DOI** 10.1002/pssa.200521129

Evaluation of Bi–W-oxides for visible light photocatalysis

A. P. Finlayson[*, 1], **V. N. Tsaneva**[1], **L. Lyons**[2], **M. Clark**[2], and **B. A. Glowacki**[1]

[1] Department of Materials Science and Metallurgy, University of Cambridge, Pembroke Street, Cambridge CB2 3QZ, United Kingdom
[2] Bentham Instruments Ltd, 2 Boulton Road, Reading RG2 0NH, United Kingdom

Received 6 July 2005, accepted 2 November 2005
Published online 5 December 2005

PACS 61.10.Nz, 78.30.Fs, 78.40.Fy, 82.47.Jk

Photocatalytic solar water splitting has the potential to become a low-carbon source of hydrogen fuel over the coming decades if the issue of low visible light absorption can be addressed without sacrificing chemical stability. We report on an investigation into the potential of the Bi–W-oxides, Bi_2WO_6 and Bi_6WO_{12}, as visible light photocatalysts. X-ray diffraction and Raman spectroscopy have been used to assess the structure of the oxides, whilst UV–vis diffuse reflectance spectroscopy analysed with the Kubelka–Munk function has been used to identify their optical band gaps. It has been revealed that Bi_6WO_{12} shows significantly higher optical absorption in the region above 440 nm than either Bi_2O_3 or WO_3, raising the possibility of enhanced photocatalytic activity under solar illumination. Bi_2WO_6 has a marginally lower band gap at 2.59 eV than Bi_2O_3 or WO_3 but the results reported herein raise doubts concerning its chemical stability under aqueous, illuminated conditions for protracted periods of time.

1 Introduction

Photocatalysis was first demonstrated in 1972 when Fujishima used a TiO_2 photoanode to split water with the aid of ultra-violet light [1]. Since then, a wide range of photocatalytically active systems have been discovered and developed into a range of devices for water purification, environmental cleaning, and solar energy conversion within dye-sensitised solar cells. However, the original aim of efficient solar water splitting remains unrealised. In common with other solar energy conversion systems, the theoretical maximum efficiency of water splitting photoelectrochemical cells is thermodynamically constrained by the Shockley–Queisser limit. For a single band gap device illuminated by terrestrial solar irradiation this implies a maximum efficiency of 30% for a band gap of 1.1 eV [2]. A photocatalyst with a band gap deviating from this optimum value will have a lower thermodynamic efficiency, thus pure TiO_2 with a gap of 3.2 eV necessarily only converts a small portion of the incident solar energy into the chemical energy of catalytic products.

It has been estimated that a minimum band gap of 1.7 eV is required to bridge the redox potentials of the water splitting reaction and reaction over-potentials, so allowing the photocatalytic reaction to proceed. Practically, those semiconducting compounds such as TiO_2 which are stable under illuminated, aqueous conditions have band gaps significantly in excess of this value. Band gap reduction through cation and, more recently, anion doping without sacrificing stability has been a focus of efforts to improve efficiency. Despite the recent successes obtained via nitridation [3] the absorption edge of TiO_2 remains towards the blue end of the visible spectrum indicating a band gap significantly exceeding the target value of 1.7 eV for efficient solar water splitting.

[*] Corresponding author: e-mail: apf23@cam.ac.uk, Phone: +44 (0)1223 762966, Fax: +44 (0)1223 334567

Both WO_3 and Bi_2O_3 based compounds have attracted some investigation as potential photocatalysts for hydrogen generation [4, 5]. They have demonstrated good chemical stability and have band gaps lower than that of TiO_2, but still significantly larger than the optimum value. It is known that a variety of intermediate oxides exhibiting different but related crystal structures exist in the Bi_2O_3–WO_3 psuedo-binary phase system, including $Bi_2W_2O_9$, Bi_2WO_6, Bi_4WO_9, Bi_6WO_{12} and the sillenite, $Bi_{14}WO_{24}$ [6]. This work has concentrated upon assessing the viability of using two of these Bi–W-mixed oxide compounds as photocatalysts by measuring the variation of band gap and chemical stability with composition.

2 Methods

2.1 Sample preparation

Bi_2O_3 (Aldrich, 99.9%) and WO_3 (Alfa Aesar, 99.8%) were obtained commercially for use as starting materials. These powders were mixed in the correct stoichiometric ratios to form Bi_2WO_6 and Bi_6WO_{12} with 10% glycerol by mass (Fisher Scientific). The pastes were spread onto alumina slides and heated under an oxygen atmosphere for 10 hours at 1173 K before cooling in air. In order to ensure a micron-scale particle size and random orientation for characterisation the sintered powders were crushed by hand until fine.

The chemical stability of the four compounds under the conditions of interest for photocatalysis was assessed by placing a small quantity of the powder in a sealed glass bottle of deionised water and exposing it to natural lighting conditions for 14 days at room temperature. Following this, the unstoppered samples were held at 60 °C for 7 days until all of the water had evaporated. Samples of exposed and unexposed powder were characterised structurally in parallel to determine the extent of deterioration as a result of this procedure. The intention of this test was to ascertain the stability of these compounds under typical reaction conditions and, therefore, no attempt was made to deposit a metallic co-catalyst nor to detect any reaction products following the exposure to illuminated aqueous conditions.

2.2 Structural characterisation

Both powder X-ray diffraction and Raman spectroscopy have been used to identify and quantify the crystal structures present in each sample.

Powder X-ray diffraction patterns were collected using unfiltered Cu K_α radiation and the Bragg–Brentano geometry over the 2θ range 20–70°. Initially, the measured patterns were matched to standard powder diffraction patterns to determine which phases were present. Quantitative analysis of sample composition and lattice parameters was performed using the Rietveld method as implemented by the Philips X'pert software [7, 8].

Raman spectroscopy was undertaken using a Renishaw Raman Microscope with a λ = 514.5 nm laser. In order to avoid sample damage the laser was operated at 6.25 mW and a large spot size (×5 magnification) was used to ensure good sampling statistics over the powder particles.

2.3 Optical characterisation

UV–vis diffuse reflectance measurements were taken using a 10 cm $BaSO_4$-coated integrating sphere attachment and a dual light source (100 W halogen/30 W deuterium lamps). Measurements were collected over the wavelength range 330 nm to 850 nm. Samples were tested both with and without a light trap to exclude the specular reflectance signal, but this was found to have a negligible effect upon the position of the optical absorption edge so only those measurements including the specular reflectance are reported herein.

The Kubelka–Munk equation (1) was used to calculate optical absorbance curves for each sample. R denotes the relative reflectance of the sample compared to a spectralon diffuse reflectance standard

$$F(R) = \frac{(1-R)^2}{2R}. \tag{1}$$

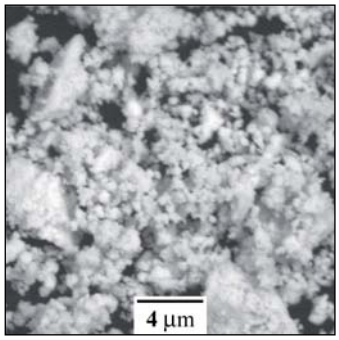

Fig. 1 Backscattered SEM micrograph of WO_3 powder showing agglomeration and wide variation in grain size.

These curves were used to construct Tauc plots of $(F(R)\cdot h\nu)^n$ against photon energy. A sample with a direct band gap will show a linear region of the curve if $n = \frac{1}{2}$, whilst an indirect band gap will exhibit a linear region if $n = 2$. In each case the band gap is given by the intersection of the extrapolated the linear portion of the plot with the energy axis [9].

3 Results

3.1 WO_3

Figure 1 shows an SEM micrograph of the fresh WO_3 powder containing a number of sub-micron particles in addition to larger particles. X-ray diffraction patterns obtained from this pure WO_3 powder and a sample exposed to illuminated aqueous conditions are contained in Fig. 2a. They indicate the presence of monoclinic WO_3 (JSPDS #71-2141). A single phase Rietveld refinement using the corresponding crystal structure (ICSD #014332) shows fair intensity matching with χ^2 equal to 34.9, consistent with an untextured powder sample. This is confirmed by the Raman spectra obtained from the same samples in Fig. 2b which are consistent with the characteristic stretching frequencies of monoclinic WO_3 reported

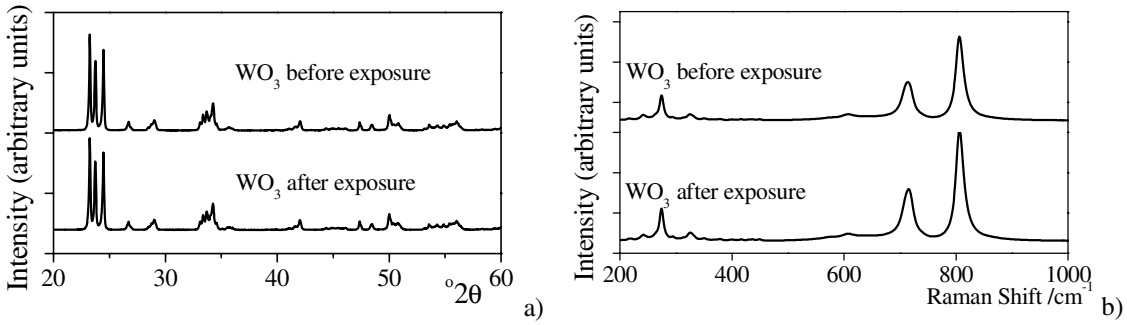

Fig. 2 a) XRD spectra and b) Raman spectra from WO_3 powder before and after exposure to illuminated, aqueous environment. Both show the presence of crystalline monoclinic WO_3.

Table 1 Rietveld refinement of WO_3 X-ray diffraction data before and after exposure to an illuminated aqueous environment.

parameter	WO_3 before exposure	WO_3 after exposure	increase (%)
a	7.308 Å	7.309 Å	+0.01
b	7.530 Å	7.531 Å	+0.01
c	10.538 Å	10.538 Å	
β	133.16°	133.16°	
χ^2	34.9	29.6	

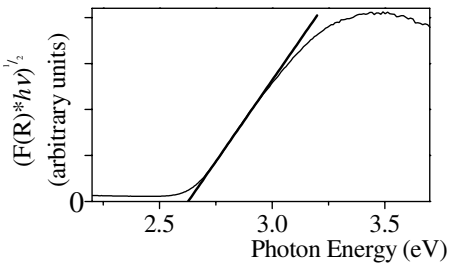

Fig. 3 Tauc plot ($n = \frac{1}{2}$) for fresh WO_3 powder. The linear extrapolation of the Tauc region (bold) intersects the energy axis at 2.63 eV.

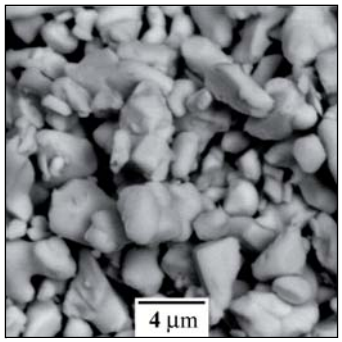

Fig. 4 Backscattered SEM micrograph of Bi_2O_3 powder showing agglomeration and wide variation in grain size.

by Hardcastle et al. [10]. Table 1 compares structural parameters of WO_3 before and after exposure to an illuminated aqueous environment as determined by Rietveld refinement of the relevant X-ray powder diffraction patterns. No significant variation in the lattice parameters *a*, *b*, *c* and *β* of monoclinic WO_3 were observed between the fresh and exposed samples. Thus the stability of this phase under such conditions is confirmed. Furthermore, no significant variation may be observed between the Raman spectra for the fresh and exposed samples. In particular, the stretching modes of terminal and bridging oxygens within tungsten oxide hydrate structures observed at 948–960 cm^{-1} and at 645–700 cm^{-1} respectively by Daniel et al. [11] are not observed in the exposed samples.

Figure 3 shows the Tauc plot derived from UV–vis reflectance measurement of fresh WO_3 samples, indicating a direct band gap of 2.63 eV ± 0.01 eV which may be compared to an experimental value of 2.8 eV reported previously [12].

3.2 Bi_2O_3

Figure 4 shows an SEM micrograph of the fresh Bi_2O_3 powder containing a number of agglomerated micron-scale particles. X-ray diffraction patterns obtained from this pure Bi_2O_3 powder and a sample exposed to illuminated aqueous conditions are contained in Fig. 5a. They reveal the presence of monoclinic α-Bi_2O_3 (JSPDS #71-0256). A single phase Rietveld refinement using the corresponding crystal structure (ICSD #002374) shows fair intensity matching with χ^2 equal to 29.8, consistent with an untextured powder sample.

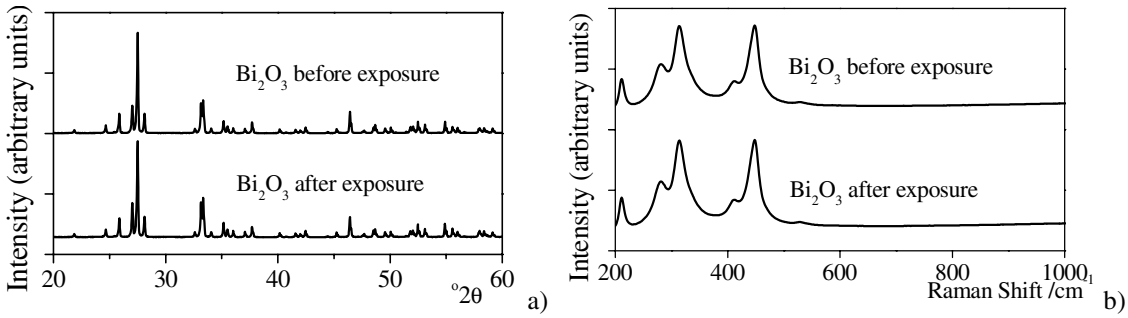

Fig. 5 a) XRD spectra and b) Raman spectra from Bi_2O_3 powder before and after exposure to illuminated, aqueous environment. Both show the presence of crystalline monoclinic α-Bi_2O_3.

Table 2 Rietveld refinement of Bi_2O_3 X-ray diffraction data before and after exposure to an illuminated aqueous environment.

parameter	Bi_2O_3 before exposure	Bi_2O_3 after exposure	increase (%)
a	5.847 Å	5.848 Å	+0.02
b	8.166 Å	8.168 Å	+0.03
c	7.510 Å	7.511 Å	+0.01
β	112.99°	112.99°	
χ^2	29.8	23.4	

This is confirmed by the Raman spectra obtained from the same samples in Fig. 5b which show the characteristic pattern of monoclinic α-Bi_2O_3 as observed by Betsch and White [13]. Table 2 compares structural parameters of Bi_2O_3 before and after exposure to an illuminated aqueous environment as determined by Rietveld refinement of the relevant X-ray powder diffraction patterns. No significant variation in either the monoclinic α-Bi_2O_3 lattice parameters (*a*, *b*, *c* and *β*) or the Raman peaks was observed between the fresh and exposed samples. Thus the stability of this phase under such conditions is confirmed.

Figure 6 shows the Tauc plot derived from UV–vis reflectance measurement of fresh Bi_2O_3 samples, indicating a direct band gap of 2.76 eV ± 0.01 eV. This value is in close agreement with the electronic structure calculated *ab initio* by Carlsson et al. which predicts an indirect band gap of 2.6 eV and an energy gap of 2.7 eV at the Γ-point [14].

3.3 Bi_2WO_6

Figure 7 shows an SEM micrograph of the fresh Bi_2WO_6 powder containing a number of sub-micron particles in addition to larger particles. X-ray diffraction patterns obtained from this powder and a sample exposed to illuminated aqueous conditions are contained in Fig. 2a. They indicate the presence of three phases: orthorhombic Bi_2WO_6 (JSPDS #79-2381), orthorhombic $Bi_2W_2O_9$ (JSPDS #89-8114) and tetragonal $Bi_7WO_{13.5}$ (JSPDS #85-1286). The presence of two additional phases, one relatively bismuth rich and the other tungsten rich, is assumed to be a consequence of incomplete solid state diffusion during the heat treatment process.

A multi-phase Rietveld refinement using the corresponding crystal structures (ICSD #067647, #088428 and #062803, respectively) shows good intensity matching with χ^2 equal to 3.6 for the unex-

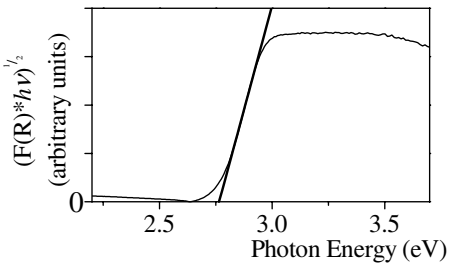

Fig. 6 Tauc plot ($n = \frac{1}{2}$) for fresh Bi_2O_3 powder. The linear extrapolation of the Tauc region (bold) intersects the energy axis at 2.76 eV.

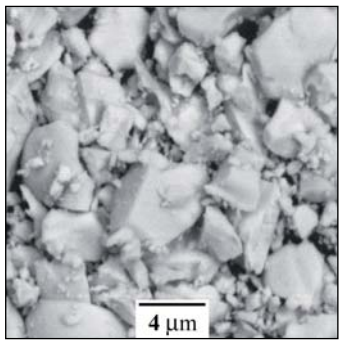

Fig. 7 Backscattered SEM micrograph of Bi_2WO_6 powder.

Table 3 Rietveld refinement of Bi_2WO_6 X-ray diffraction data before and after exposure to an illuminated aqueous environment.

parameter	Bi_2WO_6 before exposure	Bi_2WO_6 after exposure	increase (%)
a (Bi_2WO_6)	5.437 Å	5.435 Å	+0.04
b (Bi_2WO_6)	16.432 Å	16.431 Å	+0.01
c (Bi_2WO_6)	5.458 Å	5.457 Å	+0.02
wt% (Bi_2WO_6)	85.9	81.1	−5.6
a ($Bi_2W_2O_9$)	5.433 Å	5.432 Å	−0.02
b ($Bi_2W_2O_9$)	5.415 Å	5.411 Å	+0.07
c ($Bi_2W_2O_9$)	23.700 Å	23.685 Å	+0.06
wt% ($Bi_2W_2O_9$)	10.7	14.0	+30.8
a ($Bi_7WO_{13.5}$)	12.501 Å	12.499 Å	−0.02
c ($Bi_7WO_{13.5}$)	11.235 Å	11.224 Å	−0.10
wt% ($Bi_7WO_{13.5}$)	3.4	4.8	+41.2
χ^2	3.6	12.6	

posed sample. Table 3 compares structural parameters of Bi_2WO_6 before and after exposure to an illuminated aqueous environment as determined by Rietveld refinement of the relevant X-ray powder diffraction patterns. The exposed sample has a significantly higher χ^2 value and the weight fraction of Bi_2WO_6 has decreased to from 85.9 wt% to 81.1 wt% accompanied by corresponding increases in the weight fractions of the two minority phases. Taken with the observation that the Rietveld fitting parameters for the exposed sample indicate that those peaks and only those peaks attributed to Bi_2WO_6 have an increased width compared to the fresh sample, it is possible that this reflects the partial amorphisation of Bi_2WO_6 under these conditions.

Figure 2b shows Raman spectra obtained from the same samples. There are no significant differences before and after exposure to an illuminated aqueous environment and the peaks present may be matched to previously reported spectra for Bi_2WO_6 [15]. The absence of new Raman bands implies the absence of a strongly Raman-active hydrated phase formed following the exposure.

Figure 9 shows the Tauc plot derived from UV–vis reflectance measurement of fresh Bi_2WO_3 samples, indicating a direct band gap of 2.59 eV ± 0.01 eV compared to a value of 2.69 eV estimated by a previous study into the photocatalysis of Bi_2WO_6 [16].

3.4 Bi_6WO_{12}

Figure 10 shows an SEM micrograph of the fresh Bi_6WO_{12} powder illustrating the wide variation in particle size and the highly angular shape of the particles in this sample. X-ray diffraction patterns ob-

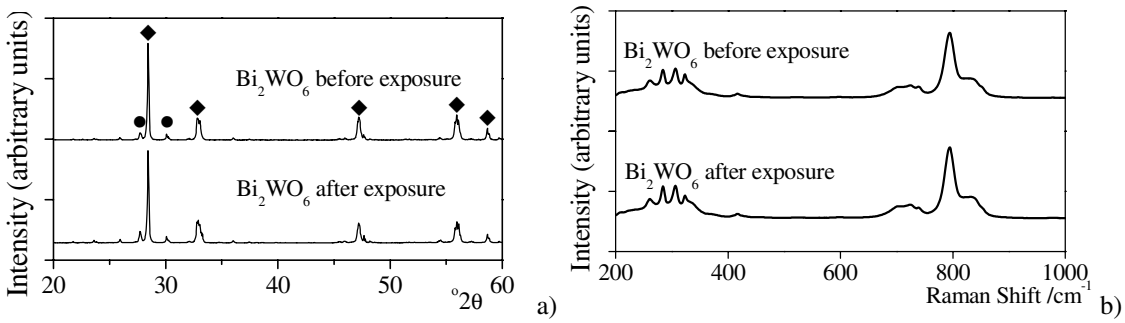

Fig. 8 a) XRD spectra and b) Raman spectra from Bi_2WO_6 powder before and after exposure to illuminated, aqueous environment. Diamonds indicate features characteristic of Bi_2WO_6 and circles those characteristic of $Bi_4W_5O_{21}$.

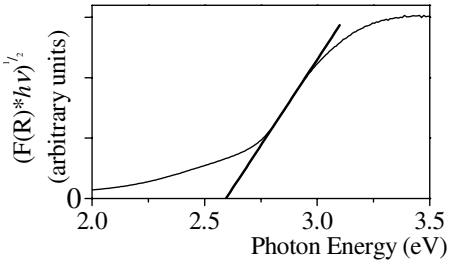

Fig. 9 Tauc plot ($n = \frac{1}{2}$) for fresh Bi_2WO_6 powder. The linear extrapolation of the Tauc region (bold) intersects the energy axis at 2.59 eV.

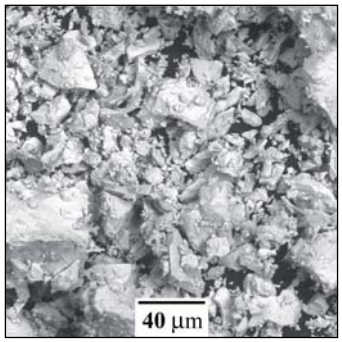

Fig. 10 Backscattered SEM micrograph of Bi_6WO_{12} powder showing very wide variation in the size of the angular grains.

tained from this sample before and after exposure to illuminated aqueous conditions are contained in Fig. 11a. They indicate the presence of three phases: tetragonal $Bi_{5.8}WO_{11.56}$ (JSPDS #89-8516), orthorhombic Bi_2WO_6 (JSPDS #79-2381) and tetragonal $Bi_{14}WO_{24}$ (JSPDS #89-6666). Again, the presence of two additional phases, one relatively bismuth rich and the other tungsten rich, is assumed to be a consequence of incomplete solid state diffusion during the heat treatment process.

Examination of the $Bi_2O_3-WO_3$ pseudo-binary phase diagram [6] reveals the presence of a solid solution region extending from $Bi_5WO_{10.5}$ to $Bi_7WO_{13.5}$ below 1147 K. These compounds share a common structure and are distinguished by differing site occupancies of Bi^{3+} and W^{6+} upon a subsection of the cation sites and different degrees of anion site occupancy and disorder to maintain overall charge neutrality. Thus the X-ray scattering of these compounds is sufficiently similar that they cannot be unambiguously distinguished by the current method and whilst the standard structure $Bi_{5.8}WO_{11.56}$ (ICSD #88840) has been used it would be erroneous to assume a Bi/W ratio of 5.8 as the data merely support the statement: $5 < Bi/W < 7$.

A multi-phase Rietveld refinement using appropriate crystal structures (Bi_2WO_6 ICSD #067647 and $Bi_{14}WO_{24}$ ICSD #062803) shows good intensity matching with χ^2 equal to 8.3 for the unexposed sample. Table 4 compares structural parameters of Bi_6WO_{12} before and after exposure to an illuminated aqueous environment. Again, the exposed sample has a significantly higher χ^2 value and a decreased weight fraction of Bi_2WO_6, as was observed in the Bi_2WO_6 samples. It is also worthy of note that there is an unusually large decrease in the $Bi_{5.8}WO_{11.56}$ *c* lattice parameter in both Bi_2WO_6 and Bi_6WO_{12} samples.

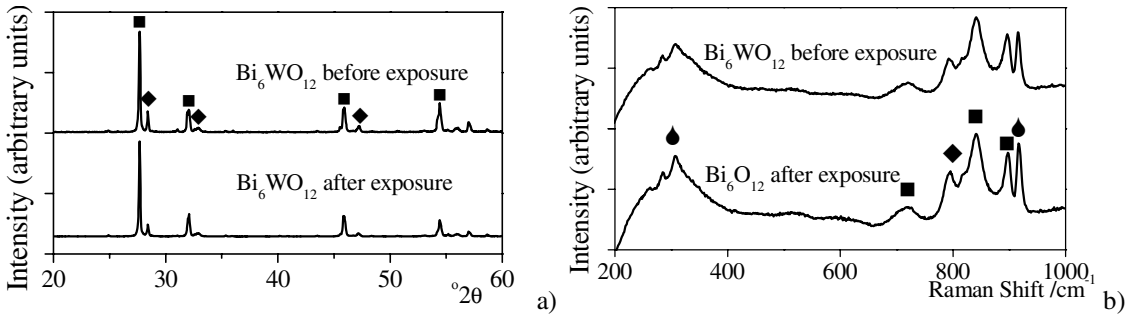

Fig. 11 a) XRD spectra and b) Raman spectra from Bi_6WO_{12} powder before and after exposure to illuminated, aqueous environment. Squares indicate features characteristic of $Bi_7WO_{13.5}$, diamonds those characteristic of Bi_2WO_6 and teardrops those characteristic of $Bi_{14}WO_{24}$.

Table 4 Rietveld refinement of Bi_6WO_{12} X-ray diffraction data before and after exposure to an illuminated aqueous environment.

parameter	Bi_6WO_{12} before exposure	Bi_6WO_{12} after exposure	increase (%)
a ($Bi_{5.8}WO_{11.56}$)	12.510 Å	12.508 Å	−0.02
c ($Bi_{5.8}WO_{11.56}$)	11.240 Å	11.231 Å	−0.08
wt% ($Bi_{5.8}WO_{11.56}$)	75.0	75.4	−0.5
a (Bi_2WO_6)	5.438 Å	5.437 Å	−0.02
b (Bi_2WO_6)	16.437 Å	16.431 Å	−0.04
c (Bi_2WO_6)	5.459 Å	5.458 Å	−0.02
wt% (Bi_2WO_6)	17.5	15.2	−13.1
a ($Bi_{14}WO_{24}$)	8.709 Å	8.705 Å	+0.05
c ($Bi_{14}WO_{24}$)	17.353 Å	17.358 Å	+0.03
wt% ($Bi_{14}WO_{24}$)	7.4	9.4	+27.0
χ^2	8.3	15.3	

The Raman spectra obtained from the same samples are presented in Fig. 2b. Both spectra contain peaks identifiable from the spectra previously observed for Bi_7WO_{14}, Bi_2WO_6 and $Bi_{14}WO_{24}$ [14]. Figure 3 shows the Tauc plot derived from UV–vis reflectance measurement of fresh Bi_6WO_{12}, indicating an indirect band gap of 2.89 eV ± 0.01 eV.

4 Discussion

Neither of the two mixed oxide samples investigated over the course of this study was found to be pure although a few meaningful conclusions concerning bulk properties may be drawn from samples 75% pure as shown by the good agreement between those band gaps previously reported in the literature and those measured here for the same compounds. Further investigations will make use of longer heat treatments and smaller particle sizes to obtain higher quality material for investigation.

Figure 13 compares the diffuse reflectance as a function of wavelength for the four samples investigated. It is readily apparent that only Bi_6WO_{12} extends the absorption significantly into the visible region compared with WO_3 and Bi_2O_3. However, its absolute absorption at shorter wavelengths is lower than for either parent compound, possibly as a consequence of its indirect band gap. It remains to be tested whether these lower energy photons produce catalytically active sites following absorption.

Of the four compounds investigated, Bi_2WO_6 demonstrated the lowest band gap but a low absolute absorption and a sharp optical absorption edge combine to give little absorption above 450 nm. To the

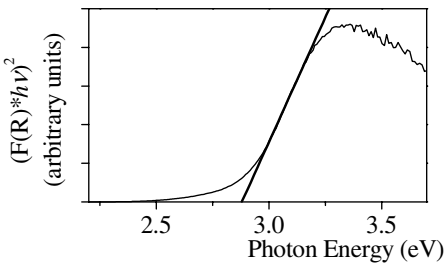

Fig. 12 Tauc plot (n = 2) for fresh Bi_6WO_{12} powder. A linear extrapolation of the Tauc region (bold) intersects the energy axis at 2.89 eV.

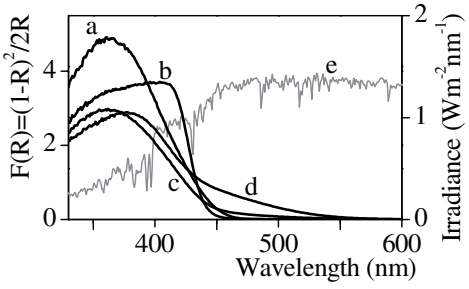

Fig. 13 Measured UV–vis diffuse reflectance curves for a) WO_3, b) Bi_2O_3, c) Bi_2WO_6, and d) Bi_6WO_{12} compared to e) reference solar spectral irradiance (air mass 1.5) [17].

best of our knowledge there have been no studies performed into the long term stability of Bi_2WO_6 in aqueous environments. However, in the light of the structural differences and possible amorphisation observed here following exposure to an illuminated aqueous environment this is an important issue which must be addressed further if Bi_2WO_6 it is to be used as a photocatalyst over longer timeframes than used in the chemical laboratory.

5 Conclusion

The feasibility of preparing Bi–W-oxides via a paste-based route has been demonstrated. This opens the possibility of using viscous processing techniques such as micro-coextrusion as explored previously [18]. It follows that a more exhaustive study might benefit from the greater control over sample composition and accelerated sample deposition for heat treatment optimisation allowed by these techniques.

Even in a relatively impure sample, Bi_6WO_{12} shows promise as a photocatalyst exhibiting enhanced visible light absorption compared to Bi_2O_3 or WO_3 and good chemical stability. The possible amorphisation of Bi_2WO_6 under aqueous, illuminated conditions casts doubt over its future application as a photocatalyst.

Acknowledgement A. P. Finlayson acknowledges the support of the Engineering and Physical Sciences Research Council throughout the duration of this investigation.

References

[1] A. Fujishima and K. Honda, Nature **238**, 37 (1972).
[2] W. Shockley and H. J. Quiesser, J. Appl. Phys. **32**(3), 510 (1961).
[3] R. Asahi, T. Morikawa, T. Ohwaki, K. Aoki, and Y. Taga, Science **293**, 269 (2001).
[4] K. Gurunathan, Int. J. Hydrog. Engergy **29**, 933 (2004).
[5] G. R. Bamwenda and H. Arakawa, Appl. Catal. A **210**, 181 (2001).
[6] E. I. Speranskaya, Neorg. Mater. **6**(1), 149 (1970).
[7] D. B. Wiles and R. A. Young, J. Appl. Crystallogr. **14**, 149 (1981).
[8] L. B. McCusker, R. B. von Dreele, D. E. Cox, D. Louer, and P. Scardi, J. Appl. Crystallogr. **32**, 36 (1999).
[9] J. Tauc, R. Grigorovici, and A. Vancu, phys. stat. sol. **15**, 627 (1966).
[10] F. D. Hardcastle and I. E. Wachs, J. Raman Spectrosc. **26**(6), 397 (1995).
[11] M. F. Daniel, B. Desbat, J. C. Lassegues, B. Gerand, and M. Figlarz, J. Solid State Chem. **67**, 235 (1987).
[12] B. Ingham, S. V. Chong, and J. L. Tallon, Curr. Appl. Phys. **4**, 202 (2004).
[13] R. J. Betsch and W. B. White, Spectrochim. Acta A **34**, 505 (1978).
[14] J. M. Carlsson, B. Hellsing, H. S. Domingos, and P. D. Bristowe, Phys. Rev. B **65**, 205122 (2002).
[15] F. D. Hardcastle and I. E. Wachs, J. Raman Spectrosc. **26**(6), 407 (1995).
[16] J. Tang, Z. Zhou, and J. Ye, Catal. Lett. **92**(1/2), 53 (2004).
[17] ASTM G 170-03, ASTM International (2003).
[18] A. P. Finlayson, E. Ward, V. N. Tsaneva, and B. A. Glowacki, J. Power Sources **145**(2), 667 (2005).

